Journal of
Materials Chemistry A

Accepted Manuscript

This article can be cited before page numbers have been issued, to do this please use: Z. Peng, X. Liu, H. Lin, Z. Wang, Z. Li, B. Li, Z. Liu and S. Liu, *J. Mater. Chem. A*, 2016, DOI: 10.1039/C6TA08529F.

This is an *Accepted Manuscript*, which has been through the Royal Society of Chemistry peer review process and has been accepted for publication.

Accepted Manuscripts are published online shortly after acceptance, before technical editing, formatting and proof reading. Using this free service, authors can make their results available to the community, in citable form, before we publish the edited article. We will replace this *Accepted Manuscript* with the edited and formatted *Advance Article* as soon as it is available.

You can find more information about *Accepted Manuscripts* in the Information for Authors.

Please note that technical editing may introduce minor changes to the text and/or graphics, which may alter content. The journal's standard Terms & Conditions and the Ethical guidelines still apply. In no event shall the Royal Society of Chemistry be held responsible for any errors or omissions in this *Accepted Manuscript* or any consequences arising from the use of any information it contains.

ROYAL SOCIETY OF CHEMISTRY

www.rsc.org/materialsA

View Article Online
DOI: 10.1039/C6TA08529F

Journal Name

PAPER

Surface engineering on a nanocatalyst: basic zinc salt nanoclusters improve catalytic performances of Ru nanoparticles

Received 00th January 20xx,
Accepted 00th January 20xx

DOI: 10.1039/x0xx00000x

www.rsc.org/

Zhikun Peng, Xu Liu, Huinan Lin, Zhuo Wang, Zhongjun Li, Baojun Li,* Zhongyi Liu* and Shouchang Liu

Herein, we report a novel surface-modified Ru-based catalysts with chemisorption of basic zinc sulfate salts ($3Zn(OH)_2{\cdot}ZnSO_4{\cdot}xH_2O$, BZSS) and demonstrate their enhanced selectivity toward cyclohexene (CHE) in benzene-selective hydrogenation. BZSS nanoclusters are confirmed to regulate surface and electronic properties on Ru nanoparticles. The surface active sites on Ru nanoparticles are reconstructed because the strong active sites are selectively occupied and blocked by BZSS nanoclusters. Lewis acid active sites, which are introduced by BZSS and modified by the interaction between Ru(0) and BZSS, can retain the activity of Ru catalyst and greatly improve the selectivity toward CHE. Benefiting from the BZSS nanoclusters located on the Ru nanoparticles, the surface-modified catalysts present excellent selectivity with high activity for the hydrogenation reaction and. This is particularly clear in that the catalyst operated stably for more than 600 h on an industrial production line; the benzene conversion was maintained at 40%, and the selectivity toward CHE was maintained over 80%.

1. Introduction

In the last decade, many metal nanoparticles (NPs) with specific size, shape, and crystalline phase were successfully prepared.[1-3] These metal NPs possess special electron orbit, high surface energy, and abundant surface defects. As a result, these novel metal NPs present superior catalytic activities and correspond to their bulk counterparts regarding many important reactions and significant breakthroughs.[4-7] When accompanied by the high activity, the metal NPs are apt to gradually lose their activities during cycling caused by serious aggregation under harsh working conditions.[8] It is particularly difficult to obtain a satisfactory selectivity for the target intermediate products[9,10] on the disordered metal NPs.

Because these deficiencies originated from the intrinsic property of metal NPs, they cannot be overcome by a single component or structure strategy. Fortunately, introducing other heterogeneous structures to metal NPs and the use of their synergistic effect to overcome the drawbacks are effective.[11,12] Methods involving metal alloying,[9,13] atomic layer deposition,[14-16] molecular modification,[10,17-20] and core shell construction[8,21-23] have been explored. Constructing heterogeneous nanoclusters on metal NPs is one of the most promising strategies for modifying active sites, and this will have great application potential in the chemical reactions and energy environment.[24-28]

Benzene-selective hydrogenation is of great significance for both scientific research and practical applications.[29-31] This is especially true because the cost-efficient synthesis of the intermediate (cyclohexene, CHE) facilitates subsequent synthesis such as hydration to cyclohexanol and further to adipic acid and ε-caprolactam. Due to successful benzene-selective hydrogenation to CHE, the normal cyclohexane oxidation, dehydration of cyclohexanol, and dehalogenation of cyclohexane halide steps can be eliminated.[32,33]

Currently, Ru-based catalysts are the most effective.[34] Nevertheless, under common conditions, the intermediate of stepwise hydrogenation of benzene is barely formed due to the free standard reaction enthalpies (benzene → CHE: −23 kJ mol^{-1} and CHE → cyclohexane (CHA): −75 kJ mol^{-1}).[35] Due to the severe thermodynamic limitations, this challenging reaction is a perfect probe reaction to evaluate catalyst performance. Most studies have enhanced the selectivity by employing hydrophilic support,[36-39] regulating the surface acidity of support,[40,41] decorating the primary metal with a second metal component,[29,42,43] or introducing various kinds of additives such as inorganic[44-46], organic additives,[47-51] or ionic liquids[35,52-54] to regulate the hydrophilicity and the electronic properties of Ru NPs. Although these approaches have been somewhat effective, further promotion of their activity, selectivity, and stability is still required.

The modification of Ru NPs catalysts with Zn or ZnO species to improve benzene-selective hydrogenation performance led to more speculations (hydrophilicity and/or synergistic effect) and optimization of the reaction conditions (mass ratio of the

School of Chemistry and Molecular Engineering, Zhengzhou University, 100 Kexue Avenue, Zhengzhou 450001, P. R. China. E-mail: liuzhongyi@zzu.edu.cn and lbjfcl@zzu.edu.cn

† Electronic Supplementary Information (ESI) available: Additional characterization results and raw reaction data are included. See DOI: 10.1039/x0xx00000x

View Article Online
DOI: 10.1039/C6TA08529F

supports, zinc content, or comparison of different preparation methods, etc.).[39,55-57] However, a deep understanding of the modification mechanism and the establishment of a new model are very urgent at this stage. These issues motivate us to explore the design and preparation of highly efficient and greener catalytic systems by locating a novel heterogeneous nanostructure on Ru NPs. This offers new fundamental insight into benzene-selective hydrogenation.

Basic zinc sulfate salt ($3Zn(OH)_2{\cdot}ZnSO_4{\cdot}xH_2O$, BZSS) is a chemical combination of alkali and acid salt, and Zn(II) species have strong hydrophilicity and adsorption abilities in the aqueous phase. The nontoxic BZSS has abundant crystal water and this makes the BZSS-modified metal NPs well dispersed in aqueous phase. BZSS can be formed by the pretreatment or reaction of Ru-Zn (Zn species as ZnO or $Zn(OH)_2$) catalysts.[42,43,57,58] Therefore, BZSS is a potential modifying agent on the surface of Ru NPs.

Herein, a novel surface-modified Ru NPs with chemisorption of BZSS were synthesized. They were employed as a catalyst in benzene-selective hydrogenation without inorganic additives (except for $ZnSO_4$) or a second metal. The BZSS is confirmed to regulate surface and electronic properties of Ru NPs. Benefiting from the BZSS nanoclusters locating on Ru NPs, the catalysts provide excellent selectivity and stability with high activity for the hydrogenation reaction.

2. Experimental section

2.1 Preparation of RuAD-based catalyst

Preparation of BZSS. The BZSS is prepared according to the following equation:

$$6NaOH + 4ZnSO_4 + xH_2O = 3Zn(OH)_2{\cdot}ZnSO_4{\cdot}xH_2O + 3Na_2SO_4 \quad (1)$$

In detail, NaOH solution (0.14 M, 150 mL) with magnetic stirring was treated with $ZnSO_4$ solution (0.14 M, 100 mL) dropwise and then agitated for 5 min. The resulting suspension (250 mL) contain 1575 mg of $3Zn(OH)_2{\cdot}ZnSO_4$ in as-prepared BZSS. The suspension is used as a BZSS source for preparing RuAD-based catalysts without separation.

Preparation of Ru NPs. Ru catalysts were prepared with a similar precipitation method according to the procedure in literature.[59] $RuCl_3{\cdot}3H_2O$ (21.62 g) was dissolved in 200 mL of H_2O with agitation. NaOH (12.36 g) was dissolved in 200 mL of H_2O and then added to the above stirred solution instantaneously; the resulting mixture was agitated for an additional 30 min. The black precipitate was then transferred into a 1 L Teflon-lined autoclave. Hydrogen was introduced into the autoclave to raise the total internal pressure of 5 MPa and operated at 150°C, 800 *rpm* for 3 h. To improve washing efficiency, when the reaction mixture was cooled, the resulting black powder was washed with hot water (55±5°C) until Cl^- was undetectable, and then the desired Ru catalyst was harvested.

Preparation of RuADX catalysts. The RuAD-based catalysts were prepared by fixing 2.0 g of Ru NPs in $ZnSO_4$ solution (0.58 M, 280 mL). For a typical preparation of Ru AD300, 47.6 mL of the as-prepared BZSS suspension and 2.0 g of Ru NPs were transferred to a 1 L Hastelloy autoclave; water was then added to adjust the $ZnSO_4$ solution to 280 mL. The mixture was kept at 50°C and stirred at 500 *rpm* for 1 h. The resultant product was filtered and washed to remove SO_4^{2-} (0.1 M $BaCl_2$ test), and subsequently vacuum-dried in oven at 60°C. The RuAD-75, 150, 300, 450, and 600 correspond to the volume of BZSS suspension of 11.9, 23.8, 47.6, 71.4, and 95.2 mL, respectively. The suspension was agitated by magnetic stirring for 1 h before being used as a BZSS source for preparing RuADX catalysts. This ensures the consistency of the amount of BZSS taken at each step (Table S1†). The obtained catalysts were denoted as RuADX, in which X means the mass of $3Zn(OH)_2{\cdot}ZnSO_4$ in as-prepared BZSS chemisorbed on 2.0 g of Ru NPs. The Zn content of the catalysts is presented in Table S2†, which indicates that the BZSS is almost quantitatively adsorbed on the Ru NPs.

2.2 Characterization

Powder X-ray diffraction (XRD) patterns were performed on a Rigaku Dmax-3C X-ray diffractometer using Cu K_α radiation (λ = 0.15418 nm) with a tube voltage of 40 kV and a current of 40 mA. The 2θ angles were scanned from 5° to 80° at $4°{\cdot}min^{-1}$. Transmission electron microscope (TEM) images and energy dispersive spectroscopy (EDS) were observed on a JEOL JEM-2011 instrument at an accelerating voltage of 200 kV. A JEOL JSM-7500F field-emission scanning electron microscope (FESEM) was used at an accelerating voltage of 5 kV. The multipoint Brunauer–Emmett–Teller surface area (S_{BET}) and porosity were measured by N_2 physisorption at 77 K on a Quantachrome NOVA 1000e instrument. The zinc content of RuADX was measured by X-ray fluorescence (XRF) on a Bruker S4 Pioneer instrument.

The H_2 chemisorption was used to determine the dispersion of Ru, which was performed on the Quantachrome Autosorb-IQ gas adsorption analyzer. The weighed sample (~100 mg) was purged with He for 30 min at room temperature and reduced at 200°C for 2 h under 10 vol.% H_2/Ar. It was then vacuumed for 2 h and cooled to 40°C. The amount of H_2 chemisorption was measured under 80, 160, 240, 320, 400, 480, 560, 640, and 720 mm Hg. The dispersion of Ru was calculated according to the H_2 uptake with the assumption of H_2:Ru stoichiometry of 1:2 and a Ru surface with an atomic density of 1.63×10^{19} atoms m^{-2}.[60]

Thermal stability of the sample in Ar was characterized by thermogravimetry-differential scanning calorimetry (TG-DSC) on a NETZSCH STA 449F3 instrument. NH_3-TPD was employed on a Quantachrome Autosorb-IQ gas adsorption analyzer. 150 mg of catalyst (35 mg of sample for BZSS) was purified at 200°C for 1 h under He and cooled to room temperature. The 10 vol.% NH_3/He mixed gas was introduced instead of He at this temperature for 1 h to ensure the saturation adsorption of NH_3. The catalyst was then purged with He for 1 h to ensure the removal of physical adsorption of NH_3. The desorption curve of NH_3 was obtained by heating the sample from 40 to 700°C at $10°C\ min^{-1}$ under He with the flow rate of 30 mL min^{-1}. For H_2-TPR measurement, 10 mg of catalyst was loaded.

View Article Online
DOI: 10.1039/C6TA08529F

The catalyst was purged in an Ar stream at room temperature. The experiment was carried out within the temperature range of 20–200°C under 10 vol.% H_2/Ar mixed gas with a flow rate of 30 mL min^{-1}. For H_2-TPD test, 150 mg of sample was loaded. The sample was reduced at 200°C for 2 h under 10 vol.% H_2/Ar, and then cooled to room temperature under Ar stream. The 10 vol.% H_2/Ar mixed gas was introduced instead of Ar at this temperature for 1 h to ensure the saturation adsorption of H_2. The sample was then purged with Ar for 1 h to ensure the removal of physical adsorption of H_2. The desorption curve of H_2 was acquired by heating the sample from 40 to 700°C at 10°C min^{-1} under Ar with a flow rate of 30 mL min^{-1}.

The nature of the acid site was characterized by the FTIR spectroscopy of adsorbed pyridine (Py-IR) on a Bruker TENSOR II spectrometer. The sample (10 mg) with KBr were ground to a fine powder and pressed into a thin self-supporting wafer. The wafer was mounted in an IR cell equipped with CaF_2 windows and evacuated at 200°C (10^{-1}–10^{-2} Pa) for 3 h. After this pretreatment, the samples were cooled to 25°C under evacuation. After the background spectrum was recorded, pyridine was introduced and balanced at this temperature for 1 h. The platelet was then evacuated at 25°C (10 min) to remove physisorbed pyridine. The spectrum was recorded with 4 cm^{-1} resolution by signal-averaging 32 scans.

The surface electronic states were determined by X-ray photoelectron spectroscopy (XPS) on a PHI Quantera SXM spectrometer with Al Kα = 1486.6 eV as excitation source where the binding energies were calibrated by referencing the C 1s peak (284.8 eV) to reduce the sample charge effect. The hydrophilicity of the catalyst surface was measured by the water contact angle using a JC2000 C1 instrument at ambient temperature. Raman spectra were detected on a LabRAM HR Evolution Raman Spectrometer.

2.3 Catalytic evaluation

With the as-prepared catalysts, the benzene-selective hydrogenation was operated in a 1 L Hastelloy autoclave. Then, 2.0 g of catalyst, 280 mL of $ZnSO_4$ aqueous solution (0.58 mol L^{-1}) was charged into the autoclave, and then sealed and purged with H_2 for three times to expel air. The water provides a soluble environment for the additive and renders a water layer around the catalyst; $ZnSO_4$ is the most effective inorganic additive to improve CHE selectivity. Both of them are effective for obtaining a desirable selectivity of CHE. [29–34,39,42,43,57,58] The stirring rate was initially fixed at 800 *rpm* with hydrogen pressure of 4.0 MPa. When the temperature reached 150°C, the line was charged with benzene (140 mL), and the hydrogen pressure was elevated to 5.0 MPa with a stirring rate of 1400 *rpm*. This is sufficient to eliminate the diffusion effects. The reaction conditions adopted here are typical for the benzene-selective hydrogenation.[42,43,58] The reaction process was monitored by discharging ~0.5 mL of the reaction mixture at periodic 5 min followed by analysis on a gas chromatography with a FID detector. Benzene, cyclohexene and cyclohexane were quantified using calibration curves. The organic was removed after the reaction, and the solid sample was washed with distilled water until no SO_4^{2-} remained. It was then vacuum-dried at 333 K for characterization. The RuADX catalysts after reaction are denoted as RuADX AH where AH stands for after hydrogenation.

To compare the intrinsic catalytic performance, the activity was expressed as the turnover frequency (TOF) of benzene. The selectivity was expressed as the S_{40}. Here, S_{40} means the value of selectivity toward CHE when benzene conversion is 40%. To calculate the TOF according to the literature,[60] we used the specific activity (r_0), and it is the moles of benzene converted per second at zero reaction time. The experimental benzene content-reaction time (t) curve was fitted with a polynomial equation, which was differentiated, and the r_0 was acquired by substituting zero for t. The TOF value was calculated using the following equation:

$$TOF = \frac{r_0 \times M_{Ru}}{dispersion \times W_{cat}} \quad (2)$$

Here, M_{Ru} and W_{cat} are the molar mass of Ru and the loading of Ru on the catalyst, respectively. The dispersion of Ru was determined by H_2 chemisorption. Since benzene cannot be hydrogenated on the BZSS nanoclusters alone, Ru is undoubtedly the primary active site for this reaction. Thus, it is suitable to use the Ru site to calculate the TOF as a good approximation. In heterogeneous catalysis it is very difficult to define exactly the nature of the active sites. Thus, comparing the TOFs on the same basis is advantageous for researchers to disclose and interpret activity difference between different catalysts.

3. Results and discussion

3.1 Bulk structure and morphology of RuADX samples

The XRD patterns of BZSS are presented in Fig. 1a. The as-prepared BZSS matches well with $3Zn(OH)_2{\cdot}ZnSO_4{\cdot}xH_2O$. The diffraction patterns of pure Ru NPs and RuADX are shown in Fig. S1†. The Ru catalyst kept its original crystal phase at a low amount of chemisorption (75 mg BZSS). This is ascribed to BZSS dispersing on the Ru surface. The appearance of the characteristic peak of BZSS at 12° starts for RuAD300, and the peak gradually increases in intensity with increasing BZSS chemisorption indicating that the BZSS nanoclusters adsorbed on Ru NPs. While the crystal water of BZSS has a little change after adsorbing on Ru NPs, Fig. 1b shows the diffraction

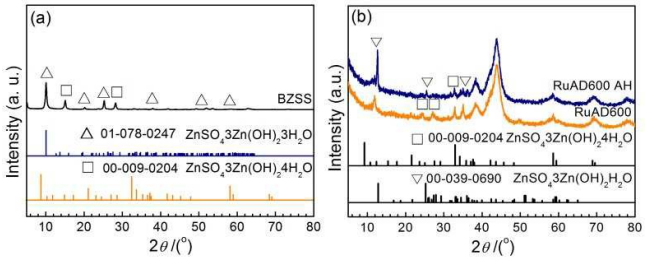

Fig. 1 The XRD patterns of (a) as-prepared BZSS and the matched standard BZSS. (b) Comparison of RuAD600 in the presence of $ZnSO_4$ before and after reaction.

View Article Online
DOI: 10.1039/C6TA08529F

patterns of RuAD600 before and after reaction. The characteristic peak of BZSS is still observed and kept after reaction confirming that the RuADX structure can be formed and maintained during reaction. This structure is important for surface engineering on catalysts to improve their catalytic performances.

The as-prepared BZSS is shown in Fig. 2a, and the adequate pores are beneficial for the adsorption and diffusion of reactant and product. The hysteresis loop in the N_2 adsorption-desorption isotherms (Fig. S2a†) also suggests the presence of mesopores in BZSS sample as further shown in the Barrett-Joyner-Halenda (BJH) pore size distribution. The typical morphology of pure Ru catalyst is shown in Fig. 2b. The dark Ru crystallite size is about 4 nm, which is consistent with the XRD results (Table S3†). The pure Ru NPs has clear edges. Nevertheless, nanoclusters appeared on Ru NPs after adsorbing BZSS (Fig. 2c and d). The nanoclusters tend to spontaneously and selectively locate on the Ru NPs.

The HRTEM image in Fig. 2e (rectangle in Fig. 2c) shows more structural details of the catalyst. The lattice fringes with the interplanar spacing of ~0.202 nm were ascribed to (101) planes of Ru NPs. The interplanar spacing of ~0.271 and ~0.276 nm around Ru NPs were ascribed to (0-22) and (-130) planes of BZSS. The EDS analysis also demonstrates that the nanoclusters existed on surface of Ru NPs are BZSS nanoclusters because the Zn, S, and O element are detected on the nanoclusters. Combined with the results of XRD, it confirms that the BZSS nanoclusters are chemisorbed on Ru NPs. Similar results are also seen in FESEM images in Fig. S3†.

The settlement test in deionized water for RuAD300 (Fig. S4†) indicates BZSS nanoclusters are not simple mechanical mixed with Ru NPs, but are a structural reconstruction caused by the interactions between the samples under the chemisorption conditions ($ZnSO_4$ solution, 50°C). These interactions lead to the transformation of BZSS from lamellar structure to nanoclusters structure, and make the

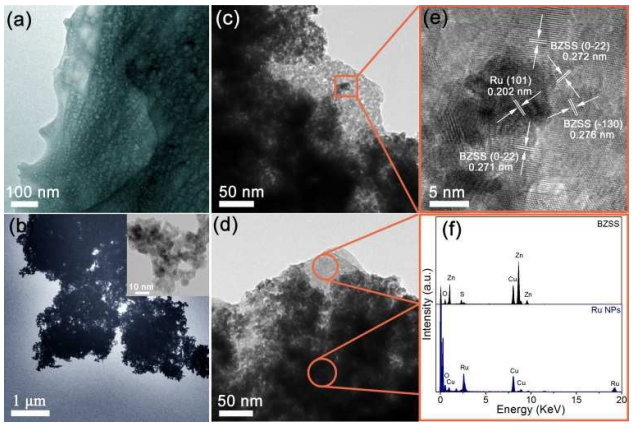

Fig. 2 TEM images of (a) as-prepared BZSS, (b) fresh Ru catalyst, the inset image is HRTEM of Ru NPs, (c, d) RuAD300, (e) HRTEM images (rectangle in c) of RuAD300 and the corresponding lattice plane of Ru and BZSS, and (f) EDS analysis of BZSS nanoclusters and Ru NPs on RuAD300.

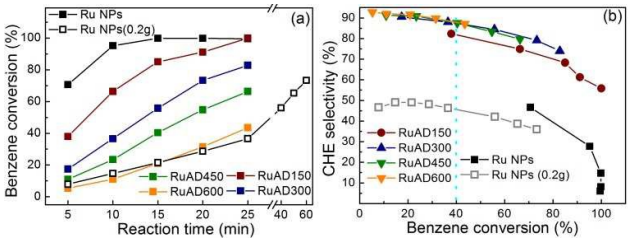

Fig. 3 Plots of the (a) conversion of benzene versus the reaction time, and (b) selectivity of CHE versus the conversion of benzene over RuADX and Ru NPs with different loadings.

nanoclusters be adsorbed and distributed on Ru NPs. A detailed description is seen in Fig. S4, ESI†.

3.2 Benzene-selective hydrogenation

Fig. 3 shows the reaction courses of benzene hydrogenation, including benzene conversion *vs.* reaction time and CHE selectivity *vs.* benzene conversion over Ru NPs and RuADX catalysts. The results show that the conversion of benzene decreased and the selectivity toward CHE increased along with the amount of chemisorbed BZSS. Over these catalysts, CHE and CHA are the only products.

Notably, Table 1 shows that the selectivity toward CHE increased greatly when chemisorbed by BZSS nanoclusters. The S_{40} (87%) of CHE on RuAD300 was identical to RuAD450 and RuAD600 but higher than that of RuAD150 (81%) and Ru NPs(0.2g, 45%). This demonstrates that Ru NPs with chemisorption of BZSS can significantly improve the CHE selectivity. When BZSS is chemisorbed up to a certain amount (300 mg), CHE selectivity is no longer increasing. Fig. 3b presents the plots of selectivity toward CHE *vs*. the conversion of benzene over these catalysts. This further confirms that BZSS significantly improved the selectivity toward CHE throughout the reaction. It is remarkable that the S_{Ymax} (the CHE selectivity recorded at the maximum yield of CHE within 25 min) toward CHE increased from 47% for Ru NPs to 87% for RuAD600. This indicates that chemisorbed BZSS changed the dynamic behavior of benzene-selective hydrogenation. The conversion of benzene at 5 min is decreased from 71% for Ru NPs to 5% for RuAD600. The TOF shows the same trend and decreases from 2.2 s^{-1} for Ru NPs to 0.2 s^{-1} for RuAD600. Versus Ru NPs, the Y_{max} increased by 85% (33% to 61%) and the TOF retain 45% (2.2 s^{-1} to 1.0 s^{-1}) on RuAD300. RuAD300 gives the highest CHE yield of 61%, making it the best result reported so far.[17,19,20]

Basically, the too strong active sites can be selectively covered by modification. As a result, the selectivity can be improved by sacrificing the activity. Fig. 3b shows that a lower conversion corresponds to a higher selectivity. Nevertheless, when lowered the loading of Ru NPs, low selectivity is still obtained along with a high TOF. These indicate that the unmodified active sites on Ru NPs are highly active to form CHA rather than CHE.

BZSS is used as catalysts for hydrogenation of benzene and

View Article Online
DOI: 10.1039/C6TA08529F

Table 1 The hydrogenation results of benzene on the RuADX.[a]

Catalyst	Conv.[b]	S_{Ymax}[c]	Y_{max}[c]	S_{40}[d]	TOF
	(%)			(%)	(s^{-1})
Ru NPs	71	47	33	n.m.[e]	2.2
Ru NPs(0.2g)	8	46	17	45	3.2
RuAD150	38	61	56	81	1.6
RuAD300	17	74	61	87	1.0
RuAD450	11	80	53	87	0.6
RuAD600	5	87	38	87	0.2

[a] Reaction condition: 2.0 g of catalyst, 280 mL of H_2O, 140 mL of benzene, 45.7 g of $ZnSO_4{\cdot}7H_2O$, temperature of 150°C, H_2 pressure of 5.0 MPa, and stirring rate of 1400 *rpm*. The raw reaction data were listed in Tables S5–10†.
[b] Benzene conversion recorded at 5 min.
[c] Values recorded at the maximum yield of CHE within 25 min.
[d] Values of selectivity toward CHE when benzene conversion is 40%.
[e] Not measured.

CHE. Table S4† indicates that pure BZSS can hardly catalyze hydrogenation of benzene or CHE. Hence, BZSS cannot act as the active sites alone for aromatics hydrogenation. In addition, Fig. S5† shows Ru NPs with chemisorption of different crystallite size of BZSS (Fig. S2b†) present similar catalytic performance. These data indicate that the crystallite size of BZSS has no obvious effects on the catalytic performance of the final catalyst.

Experiments on benzene-selective hydrogenation in the absence of $ZnSO_4$ were conducted. Compared with Ru NPs, a relatively low benzene conversion and a very high CHE selectivity are obtained for RuAD300 in the absence of $ZnSO_4$. The presence of $ZnSO_4$ can further improve the selectivity of both catalysts to some extent (Fig. S6†). A similar result by adding $ZnSO_4$ or not is observed.[58] This implies the chemisorbed BZSS can interact with ruthenium active sites and modify the Ru surface properties both in the presence and absence of $ZnSO_4$, and BZSS play a relatively primary role compared to $ZnSO_4$ in this reaction. Nevertheless, RuADX presents better catalytic performance in the presence of $ZnSO_4$.

Despite the close resemblance of the texture, the dispersion, and size of the Ru NPs (Table S3†), distinct differences in the activity and selectivity exist between the Ru NPs and RuADX catalyst. This suggests that there must be some subtle interactions between the Ru NPs and BZSS nanoclusters. Therefore, to further evaluate the synergistic effect-dependent catalytic performance, these catalysts are further characterized by XPS, Raman spectra, Py-IR, NH_3-TPD, H_2-TPR, and H_2-TPD.

3.3 Chemical state, acidic and surface properties of RuADX samples

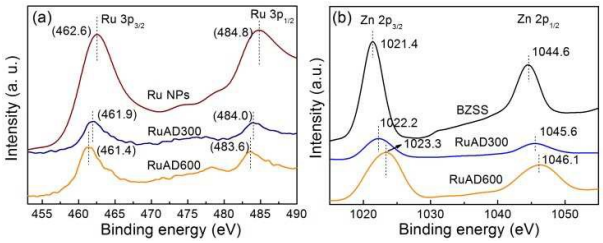

Fig. 4 Ru 3p and Zn 2p XPS spectra of Ru catalyst with different amount of adsorption of BZSS.

Ru NPs, RuAD300, and RuAD600 were selected as representative catalysts to study the electronic states of the Ru and Zn species. The Ru $3p_{3/2}$ BE of 462.6 eV and the $3p_{3/2}$–$3p_{1/2}$ doublet separation of 22.2 eV evidenced the metallic state of Ru in these catalysts.[40] After Ru chemisorbing BZSS, the BE of Ru 3p moves to the low BE side and varies with increasing BZSS chemisorption. The Ru 3d spectra also show the same tendency (Fig. S7†). A contrary variation was observed for Zn 2p moving to the high BE side with increasing adsorption of BZSS, while the BE of S 2p showed no obvious movement with chemisorption of BZSS (Fig. S7†). Apparently, the variation of BE for Ru and Zn species confirms electron transfer occurred between Ru(0) and BZSS species. It is also demonstrated electron transfer from the BZSS to the Ru 3d empty orbit. Therefore, Zn(II) species in BZSS becomes an electron-deficient species, and this interaction between Ru(0) and BZSS probably has an effect on the catalyst properties.

In BZSS ($3Zn(OH)_2{\cdot}ZnSO_4{\cdot}xH_2O$), the hydroxyl is an electron-donating group. When BZSS chemisorbed on Ru NPs, the hydroxyl electron cloud tends to migrate to Ru 3d empty orbit. This weakens the electron cloud density of the hydroxyl around Zn(II). The Zn(II) in RuADX is characterized by electron-deficient state compared with Zn(II) in pure BZSS. In the macroscopic view, it shows that Zn(II) species becomes electron-deficient and the Ru species becomes electron-rich. This electron transformation phenomenon is also discovered in other related works.[51,58]

In light of the literature,[40] the small amount of B doped in ZrO_2 samples can greatly modify the Lewis acidity of the catalysts. NH_3-TPD was employed to investigate acidity of the samples (Fig. 5). Fig. S8† shows the XRD patterns of the samples calcined at 200, 300, and 700°C in N_2 atmosphere. This indicates that the BZSS only loses part of crystal water at 200°C and decomposes to ZnO and $Zn(OH)_2$ at 300°C, which is in consistent with TGA in Fig. S9†. Therefore, it is feasible that the samples are pretreated at 200°C, and the data are discussed <300°C.

In Fig. 5a, the Ru NPs sample exhibited no desorption peaks because it has no or trace amounts of acid sites versus RuADX catalysts. Combined with the TG/DSC curves of BZSS and RuAD300 (Fig. S9†), the peaks for BZSS and RuADX at about 220-330°C are attributed to the decomposition of BZSS. The BZSS and RuADX samples exhibited a peak in the range of 50-150°C attributable to NH_3 adsorbed on weak acid sites. When Ru NPs is modified by BZSS, the RuADX samples have

View Article Online
DOI: 10.1039/C6TA08529F

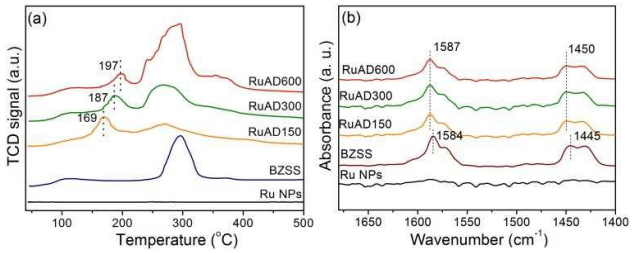

Fig. 5 (a) NH_3-TPD profiles and (b) Py-IR spectra of the samples.

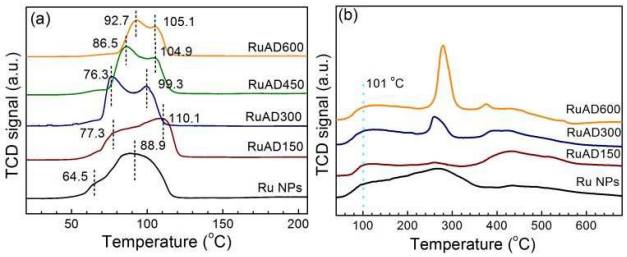

Fig. 6 (a) H_2-TPR profiles, (b) H_2-TPD profiles of Ru NPs and RuADX.

a new narrow peak at about 150-200°C indicating that a new kind of acid sites were formed. The peaks shift from 169°C for RuAD150 to 197°C for RuAD600 indicating that the acid strength increased with the amount of BZSS chemisorption. This can be explained by the electron transformation from BZSS to Ru 3d empty orbit.

Pyridine was used as a base probe to further investigate the acidic properties and acid types of the samples. According to literature[40, 61], strong Lewis acid sites-coordinated pyridine located at 1600-1630 cm^{-1} (strong L-Py), Lewis acid sites-coordinated pyridine located at 1440-1460 cm^{-1} (L-Py). For the BZSS, bands presented at 1445 and 1584 cm^{-1} belong to L-Py. The data show that BZSS contains Lewis acid sites, and it acts as a Lewis acid introduced into the Ru NPs. The BZSS showed no Brønsted acid sites at 1540 cm^{-1}.[61] Regarding RuADX samples, the L-Py bands shift to 1450, 1587 cm^{-1}, respectively. The position of the L-Py peak shifted to higher wavenumbers after BZSS chemisorption on Ru NPs. Combined with the results of XPS and NH_3-TPD, the BZSS modification induced a new kind of Lewis acid sites on Ru NPs. The Lewis acid sites are introduced by BZSS and modified by the interaction between Ru(0) and BZSS. As will be illustrated, these new Lewis acid sites can retain the activity of Ru catalyst and greatly improve the selectivity toward CHE.

Fig. 6a illustrates the hydrogen consumption of the catalysts as a function of the reduction temperature (20–200°C) during the H_2-TPR process. Reduction of all the catalysts took place in temperature range between 50°C and 122°C. The reduction peaks are characterized by two main shoulders. The shoulders are assigned step by step to the reduction of $Ru^{4+} \rightarrow Ru^{2+} \rightarrow Ru$.[58] The reduction peaks of RuADX shift to higher temperatures with increasing BZSS chemisorption, and the reduction temperatures are all higher than Ru NPs. The reduction process of ruthenium oxide appears to be retarded, this can be attributed to the electron interaction between the Ru species and BZSS. Fig. 6a shows that the low valence $Ru^{\delta+}$ compound existed as the main form in fresh Ru NPs since the second shoulder is the primary peak. With greater BZSS chemisorption, the proportion of low valence $Ru^{\delta+}$ decreases and the high valence $Ru^{\delta+}$ increases. This also reveals that the reduction process of $Ru^{\delta+}$ is changed, resulting from an electron interaction between the Ru species and BZSS.

Fig. 6b shows the H_2 desorption profiles of the chemisorbed catalysts. On fresh Ru NPs, the H_2-TPD spectra present a wide range desorption peaks from 40°C to 700°C indicating that many types of hydrogen adsorption existed on fresh Ru NPs. Therefore, the surface of Ru NPs has many active sites. Because the BZSS decomposes completely at 300°C, the desorption data are discussed <300°C. Notably, RuADX samples retain the H_2 desorption peak at about 100°C as Ru NPs, and the active sites higher than 100°C are selectively blocked by BZSS. This indicates that BZSS nanoclusters preferentially occupy the low and/or medium-temperature active sites and block the strong continuous Ru active sites. This geometric effect is beneficial for benzene-symmetric adsorption activation, which is important for CHE selectivity improvement. For RuAD150, the desorption peak between 220 and 330°C is weak. This is attributed to the coverage of the medium active sites by BZSS. It is logical to deduce that medium-temperature active sites will be gradually covered by BZSS with increasing amounts of BZSS chemisorption. The high peak signal in the range of 220-330°C for RuAD300 and RuAD600 is ascribed to the decomposition of BZSS. This indicates the active sites are regulated on Ru NPs after being modified by BZSS.

Raman spectra of Ru NPs, RuADX, and BZSS are presented in Fig. 7. There are no scattering peaks on Ru NPs. The peak for BZSS appears centered at 1180 cm^{-1}. For RuAD75, it shows two weak peaks at 846 cm^{-1} and 1040 cm^{-1} indicating that it red shifted for the Zn(II) in RuADX compared with Zn(II) in BZSS. With greater chemisorption, the peak became stronger. The variation in Raman shifts for Zn(II) species can be attributed to the interaction between Ru(0) and BZSS.

Fig. 8b illustrates the contact angle of Ru NPs and RuADX. Ru NPs exhibit hydrophobic property (contact angle > 90°). For the RuADX samples, BZSS nanoclusters introduce hydrophilic components including Zn(II) species and abundant crystal water. The hydrophilicity of Ru surface is enhanced (contact angle < 90°). When the amount of BZSS chemisorption is greater than 150 mg, the RuADX samples showed perfect wettability (contact angle ≈ 0°). In addition, BZSS-modified Ru NPs can be well dispersed in aqueous phase (Fig. S4†).

3.4 Correlation of the BZSS loadings with the catalytic performance

View Article Online
DOI: 10.1039/C6TA08529F

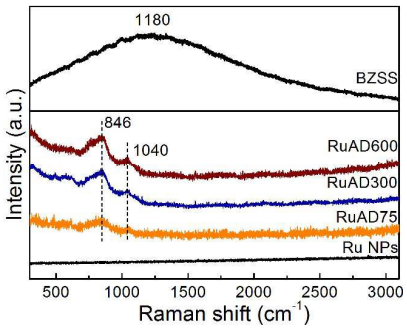

Fig. 7 Raman spectra of Ru NPs and RuADX.

By plotting the TOFs, Y_{max}, and S_{Ymax} in Table 1 against the amount of BZSS (m_{BZSS}) chemisorption, two excellent linear relationships for TOF and S_{Ymax} emerged in Fig. 8a. Unlike the positive correlation of the TOF and S_{Ymax} with m_{BZSS}, a volcano-type relationship was established for Y_{max}, indicating an optimal BZSS chemisorption to maximize the yield of CHE on Ru NPs. The highest yield of 61% was obtained on RuAD300, which is much larger than Ru NPs and other pure Ru catalysts.[35,38,56]

In light of the similarities in the composition, texture, and particle size of the RuADX catalysts shown in Table S3†, the BZSS-modified effect should be responsible for the distinct differences in catalytic performance between the Ru NPs and RuADX catalyst.

The superior behavior of the catalyst for benzene-selective hydrogenation to CHE can be explained using the mechanism illustrated in Fig. 8c. First, BZSS nanoclusters locate on Ru NPs, and they selectively chemisorb on the Ru active sites and then block the strong continuous active sites. This geometric effect reduces the probability of benzene-symmetric adsorption activation and the activity of benzene-complete hydrogenation, while increasing the proportion of the benzene-asymmetry adsorption activation and benzene-selective hydrogenation (Fig. 8c). On the other hand, the electron-rich Ru species ($Ru^{\delta-}$) and electron-deficient Zn(II) species ($Zn^{\delta+}$) originated from electron transfer between Ru(0) NPs and BZSS. Benzene with delocalized π bonds is electron-rich, and the electron-deficient Lewis acid sites should be in favor of the adsorption of benzene with the formation of electron-deficient aromatic intermediates.[40] This can be hydrogenated by spillover hydrogen (H_{so}),[62] as illustrated in Fig. 8c. Meanwhile, the interfacial $Ru^{\delta-}$ species increase the repulsive force with benzene as well as the formed CHE on Lewis acid sites and Ru NPs. These effects can retain the activity of the catalyst and improve selectivity toward CHE. At the same time, chemisorption of BZSS enhances the hydrophilicity of Ru NPs surface (Fig. 8b and Fig. S4†). This is beneficial to form a stagnant water layer on Ru surface during reaction. The hydrophilic water layer causes CHE to diffuse from catalyst surface to the organic phase, and this prevents CHE from further hydrogenation. All of these result in much higher selectivity toward CHE and retain the activity on BZSS-modified Ru NPs.

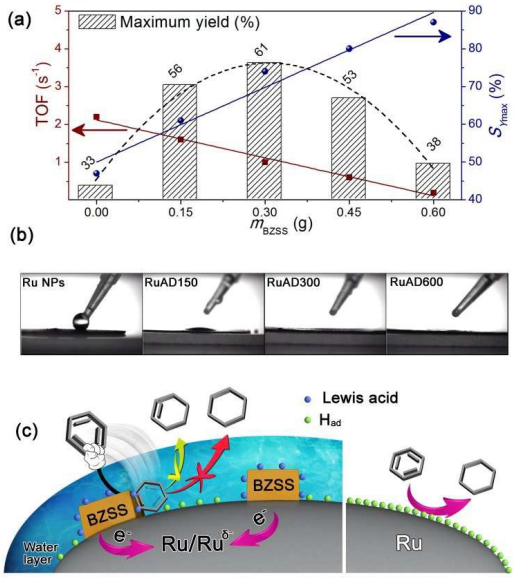

Fig. 8 (a) Correlations of TOF, S_{Ymax}, and *Y*max with the amount of BZSS chemisorption of the Ru NPs and RuADX catalysts. (b) Contact angle measurement of Ru NPs and RuADX. (c) Schematic illustration of the reaction mechanism for benzene hydrogenation on RuADX (left) and bulk Ru NPs (right).

3.5 The effect of $Zn(OH)_2$, ZnO, and NaOH in benzene-selective hydrogenation

Considering that $Zn(OH)_2$, ZnO, and NaOH can react with $ZnSO_4$ to form BZSS during reaction, the effect of $Zn(OH)_2$, ZnO, and NaOH was investigated in benzene-selective hydrogenation.

The patterns of ZnO adsorbed on Ru NPs (Fig. 9a) matched well with hexagonal phases of ZnO (JCPDS: 01-076-0704). Fig. 9b showed that BZSS diffraction peaks appear instead of ZnO phase after being treated in reaction condition. This reveals that ZnO or $Zn(OH)_2$ adsorbed on Ru NPs can react with the additive $ZnSO_4$ to form BZSS in the reaction condition. The catalytic performance of Ru NPs chemisorbed equivalent $Zn(OH)_2$ and ZnO were evaluated. Obviously, $Zn(OH)_2$ and ZnO presented exactly the same catalytic performance as RuAD300 (Table 2 and Fig. S10†). The XRD pattern of Ru NPs after treatment with NaOH in reaction condition is seen in Fig. 9c.

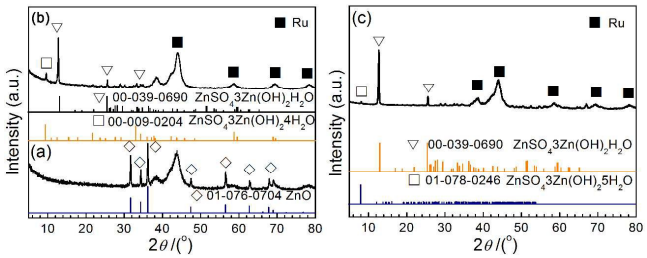

Fig. 9 The XRD patterns of (a) Ru NPs with adsorption of pure ZnO (equivalent weight of 600 mg BZSS) and (b) sample a after treatment in the reaction condition. (c) Ru NPs after treatment by adding NaOH in the reaction condition.

View Article Online
DOI: 10.1039/C6TA08529F

Table 2 The results of the equivalent modified amounts of BZSS, $Zn(OH)_2$, ZnO, and NaOH.[a]

Chemisorption composition	Catalyst	m[b]/mg	t_{40}[c]/min	t_{50}[c]/min	t_{60}[c]/min	S_{40}[d]/%	S_{50}[d]/%	S_{60}[d]/%
BZSS	Ru NPs (2.0 g)	300	11	14	16	87	85	83
$Zn(OH)_2$	a.	196	11	14	16	86	84	82
ZnO	b.	160	11	13	16	86	85	83
NaOH	c.	158	14	16	20	87	85	82

[a] The raw reaction data are listed in Tables S11–13†.
[b] The equivalent chemisorption amount compared with 300 mg BZSS, quantitative methods details are given in Table S14†.
[c] The time required when the benzene conversion is 40%, 50%, and 60%.
[d] Values of CHE selectivity when benzene conversion is 40%, 50%, and 60%.

Interestingly, NaOH in the reaction system can also react with $ZnSO_4$ to form BZSS. Adding an equivalent of NaOH also presents similar catalytic performance with RuAD300 (Table 2). Therefore, BZSS plays a key role in benzene-selective hydrogenation.

3.6 The stability operated on continuous flow reactor

The catalytic performance and stability of RuADX catalysts were carried out in a 10 m^3 capacity hastelloy continuous reaction device using RuAD300 as a representative catalyst. Long-term cycle stability of catalyst operating on an industrial production device is presented in Fig. 10. Benzene conversion was maintained at 40%, and the selectivity toward CHE was maintained higher than 80% stably for more than 600 h. The effect of the BZSS-modified Ru NPs catalyst is superior in sustaining high performance. Thus, it can not only improve the selectivity and yield of CHE in laboratory scale, but also meet the requirements of industrial production.

4. Conclusions

The novel surface-modified Ru-based catalysts with chemisorption of BZSS were synthesized and employed in benzene-selective hydrogenation. The surface-modified catalysts show much higher selectivity than Ru NPs as well as comparable activity with Ru NPs. The strong active sites on Ru NPs were selectively occupied by BZSS nanoclusters. This increased the proportion of benzene-selective hydrogenation. Lewis acid active sites, which are introduced by BZSS and modified by the interaction between Ru(0) and BZSS, can retain the activity of Ru catalyst and greatly improve the selectivity toward CHE. The geometric, electronic, and synergistic effects exist between BZSS nanoclusters and Ru NPs play a key role in benzene-selective hydrogenation. We describe the long-term cycle stability of the catalyst operating on an industrial production device. The benzene conversion was maintained at 40%, and the selectivity toward CHE was maintained more than 80% stably for more than 600 h. This strategy of locating nanoclusters on metal NPs as a proof of concept can guide design in developing heterogeneous catalysis reactions and offer significant industrial applications.

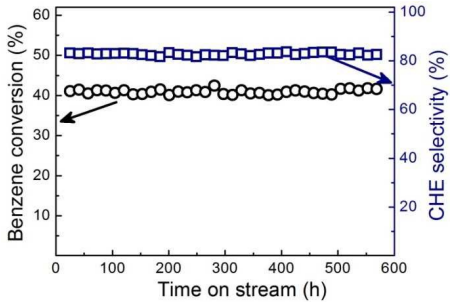

Fig. 10 The benzene conversion and CHE selectivity in industrial consecutive production process.

(Run condition: slurry bed reactor volume 10 m^3, m_{cat}/m_{BZSS}= 6–7, 0.58 mol L^{-1} $ZnSO_4$ solution, Ru/ZrO_2 = 5. $p(H_2)$ = 4.75±0.25 MPa, temperature = 140°C, stirring rate = 500 *rpm*, circulation velocity of the slurry =85 T h^{-1}, circulation velocity of benzene = 40 T h^{-1})

Acknowledgements

Financial supports from the National Natural Science Foundation of China (no. 21543011, 21273205, 21401168, U1204203) are acknowledged.

References

1 H. H. Duan, D. S. Wang and Y. D. Li, Green chemistry for nanoparticle synthesis. *Chem. Soc. Rev.*, 2015, **44**, 5778–5792.
2 Y. Wu, D. S. Wang and Y. D. Li, Nanocrystals from solutions: catalysts. *Chem. Soc. Rev.*, 2014, **43**, 2112–2124.
3 Z. B. Zhuang, Q. Peng and Y. D. Li, Controlled synthesis of semiconductor nanostructures in the liquid phase. *Chem. Soc. Rev.*, 2011, **40**, 5492–5513.
4 Y. N. Xia, Y. J. Xiong, B. Lim and S. E. Skrabalak, Shape–controlled synthesis of metal nanocrystals: simple chemistry meets complex physics? *Angew. Chem. Int. Ed.*, 2009, **48**, 60–103.
5 I. Schrader, J. Warneke, J. Backenköhler and S. Kunz, Functionalization of platinum nanoparticles with L-Proline: simultaneous enhancements of catalytic activity and selectivity. *J. Am. Chem. Soc.*, 2015, **137**, 905–912.
6 S. E. F. Kleijn, S. C. S. Lai, M. T. M. Koper and P. R. Unwin, Electrochemistry of nanoparticles. *Angew. Chem. Int. Ed.*, 2014, **53**, 3558–3586.
7 Y. Liu and W. E. Mustain, High stability, high activity Pt/ITO oxygen reduction electrocatalysts. *J. Am. Chem. Soc.*, 2012, **135**, 530–533.

View Article Online
DOI: 10.1039/C6TA08529F

8 D. Liu, W. Li, X. L. Feng and Y. Zhang, Galvanic replacement synthesis of $Ag_xAu_{1-x}@CeO_2$ (0≤x ≤1) core@shell nanospheres with greatly enhanced catalytic performance. *Chem. Sci.*, 2015, **6**, 7015−7019.

9 Z. B. Tian, Q. Y. Li, J. Y. Hou, L. Pei, Y. Li and S. Y. Ai, Platinum nanocrystals supported on CoAl mixed metal oxide nanosheets derived from layered double hydroxides as catalysts for selective hydrogenation of cinnamaldehyde. *J. Catal.*, 2015, **331**, 193−202.

10 S. T. Marshall, M. O'Brien, B. Oetter, B. Oetter, A. Corpuz, R. M. Richards, D. K. Schwartz and J. W. Medlin, Controlled selectivity for palladium catalysts using self-assembled monolayers. *Nature Mater.*, 2010, **9**, 853−858.

11 N. Tian, Z. Y. Zhou, S. G. Sun, Y. Ding and Z. L. Wang, Synthesis of tetrahexahedral platinum nanocrystals with high-index facets and high electro-oxidation activity. *Science*, 2007, **316**, 732−735.

12 C. Chen, Y. J. Kang, Z. Y. Huo, Z. W. Zhu, W. Y. Huang, H. L. Xin, J. D. S. Snyder, D. G. Li, J. A. Herron, M. Mavrikakis, M. F. Chi, K. L. More, Y. D. Li, N. M. Markovic, G. A. Somorjai, P. D. Yang and V. R. Stamenkovic, Highly crystalline multimetallic nanoframes with three-dimensional electrocatalytic surfaces. *Science*, 2014, **343**, 1339−1343.

13 Y. Pei, P. J. Guo, M. H. Qiao, H. X. Li, S. Q. Wei, H.Y. He and K. N. Fan, The modification effect of Fe on amorphous CoB alloy catalyst for chemoselective hydrogenation of crotonaldehyde. *J. Catal.*, 2007, **248**, 303−310.

14 H. J. Kim, D. H. K. Jackson, J. Lee, Y. X. Guan, T. F. Kuech and G. W. Huber, Enhanced activity and stability of TiO_2−coated cobalt/carbon catalysts for electrochemical water oxidation. *ACS Catal.*, 2015, **5**, 3463−3469.

15 N. P. Dasgupta, C. Liu, S. Andrews, F. B. Prinz and P. D. Yang, Atomic layer deposition of platinum catalysts on nanowire surfaces for photoelectrochemical water reduction. *J. Am. Chem. Soc.*, 2013, **135**, 12932−12935.

16 J. L. Lu, B. S. Fu, M. C. Kung, G. M. Xiao, J. W. Elam, H. H. Kung and P. C. Stair, Coking- and sintering-resistant palladium catalysts achieved through atomic layer deposition. *Science*, 2012, **335**, 1205−1208.

17 S. Sharma, Metal dependent catalytic hydrogenation of nitroarenes over water-soluble glutathione capped metal nanoparticles. *J. Colloid Interface Sci.*, 2015, **441**, 25−29.

18 J. J. Tan, J. L. Cui, G. Q. Ding, T. S. Deng, Y. L. Zhu and Y. W. Li, Efficient aqueous hydrogenation of levulinic acid to *γ*-valerolactone over a highly active and stable ruthenium catalyst. *Catal. Sci. Technol.*, 2016, **6**, 1469−1475.

19 R. F. Nie, H. Z. Jiang, X. H. Lu, D. Zhou and Q. H. Xia, Highly active electron-deficient Pd clusters on N-doped active carbon for aromatic ring hydrogenation. *Catal. Sci. Technol.*, 2016, **6**, 1913−1920.

20 S. R. Zhang, R. B. Jiang, Y. M. Xie, Q. F. Ruan, B. C. Yang, J. F. Wang and H. Q. Lin, Colloidal moderate-refractive-index Cu_2O nanospheres as visible-region nanoantennas with electromagnetic resonance and directional light-scattering properties. *Adv. Mater.*, 2015, **27**, 7432−7439.

21 Y. P. Xie, Z. B. Yu, G. Liu, X. L. Ma and H. M. Cheng, CdS–mesoporous ZnS core–shell particles for efficient and stable photocatalytic hydrogen evolution under visible light. *Energy Environ. Sci.*, 2014, **7**, 1895−7439.

22 X. Wang, M. Vara, M. Luo, H. Huang, A. Ruditskiy, J. Park, S. X. Bao, J. Y. Liu, J. Howe, M. F. Chi, Z. X. Xie and Y. N. Xia, Pd@Pt Core–Shell concave decahedra: a class of catalysts for the oxygen reduction reaction with enhanced activity and durability. *J. Am. Chem. Soc.*, 2015, **137**, 15036−15042.

23 F. M. Ren, H. Y. Lu, H. T. Liu, Z. Wang, Y. Wu and Y. D. Li, Surface ligand-mediated isolated growth of Pt on Pd nanocubes for enhanced hydrogen evolution activity. *J. Mater. Chem. A.*, 2015, **3**, 23660−23663.

24 S. Gao, Y. Lin, X. C. Jiao, Y. F. Sun, Q. Q. Luo, W. H. Zhang, D. Q. Li, J. L. Yang, Y. Xie, Partially oxidized atomic cobalt layers for carbon dioxide electroreduction to liquid fuel. *Nature*, 2016, **529**, 68−71.

25 H. L. Tang, J. K. Wei, F. Liu, B. T. Qiao, X. L. Pan, L. Li, J. Y. Liu, J. H. Wang and T. Zhang, Strong metal–support interactions between gold nanoparticles and nonoxides. *J. Am. Chem. Soc.*, 2016, **138**, 56−59.

26 H. L. Lin, Z. P. Shi, S. He, X. Yu, S. N. Wang, Q. S. Gao and Y. Tang, Heteronanowires of MoC–Mo_2C as efficient electrocatalysts for hydrogen evolution reaction. *Chem. Sci.*, 2016, **7**, 3399−3405.

27 Y. S.Chen, H. Choi and P. V. Kamat, Metal-cluster-sensitized solar cells. A new class of thiolated gold sensitizers delivering efficiency greater than 2%. *J. Am. Chem. Soc.*, 2013, **135**, 8822−8825.

28 S. Yusuf and F. Jiao, Effect of the support on the photocatalytic water oxidation activity of cobalt oxide nanoclusters. *ACS Catal.*, 2012, **2**, 2753−2760.

29 X. L. Zhou, H. J. Sun, W. Guo, Z. Y. Liu and S. C. Liu, Selective hydrogenation of benzene to cyclohexene on Ru-based catalysts promoted with Mn and Zn. *J. Nat. Gas Chem.*, 2011, **20**, 53−59.

30 C. Fan, Y. A. Zhu, X. G. Zhou and Z. P. Liu, Catalytic hydrogenation of benzene to cyclohexene on Ru(0001) from density functional theory investigations. *Catal Today.*, 2011, **160**, 234−241.

31 W. T. Wang, H. Z. Liu, T. B. Wu, P. Zhang, G. D. Ding and S. G. Liang, Ru catalyst supported on bentonite for partial hydrogenation of benzene to cyclohexene. *J. Mol. Catal. A-Chem.*, 2012, **355**, 174−179.

32 R. S. Suppino, R. Landers and A. J. G. Cobo, Partial hydrogenation of benzene on Ru catalysts: Effects of additives in the reaction medium. *Appl. Catal. A-Gen.*, 2013, **452**, 9−16.

33 Y. Q. Wen, X. Y. Wang, H. J. Wei, B. J. Li, P. Jin and L. M. Li, A large-scale continuous-flow process for the production of adipic acid *via* catalytic oxidation of cyclohexene with H_2O_2. *Green Chem.*, 2012, **14**, 2868–2875.

34 L. Foppa and J. Dupont, Benzene partial hydrogenation: advances and perspectives. *Chem. Soc. Rev.*, 2015, **44**, 1886−1897.

35 F. Schwab, , M. Lucas and P. Claus, Ruthenium-catalyzed selective hydrogenation of benzene to cyclohexene in the presence of an ionic liquid. *Angew. Chem. Int. Ed.*, 2011, **50**, 10453−10456.

36 P. Zhang, T. B. Wu, T. Jiang, W. T. Wang, H. Z. Liu, H. L. Fan, Z. F. Zhang and B. X. Han, Ru–Zn supported on hydroxyapatite as an effective catalyst for partial hydrogenation of benzene. *Green Chem.*, 2013, **15**, 152−159.

37 W. T. Wang, H. Z. Liu, G. D. Ding, P. Zhang, T. B. Wu, T. Jiang and

View Article Online
DOI: 10.1039/C6TA08529F

B. X. Han, Ru-Cd/Bentonite for the partial hydrogenation of benzene: a catalyst without additives. *ChemCatChem*, 2012, **4**, 1836−1843.

38 E. V. R. Fernández, J. S. Albero, A. S. Escribano and F. R. Reinoso, Effect of the metal precursor on the properties of Ru/ZnO catalysts. *Appl. Catal. A-Gen.*, 2010, **374**, 221-227.

39 S. C. Hu and Y. W. Chen, Partial hydrogenation of benzene to cyclohexene on ruthenium catalysts supported on La_2O_3–ZnO binary oxides. *Ind. Eng. Chem. Res.*, 1997, **36**, 5153−5159.

40 G. B. Zhou, Y. Pei, Z. Jiang, K. N. Fan, M. H. Qiao, B. Sun and B. N. Zong, Doping effects of B in ZrO_2 on structural and catalytic properties of Ru/B-ZrO_2 catalysts for benzene partial hydrogenation. *J. Catal.*, 2014, **311**, 393−403.

41 G. B. Zhou, J. L. Liu, X. H. Tan, Y. Pei, M. H. Qiao, K. N. Fan and B. N. Zong, Effect of support acidity on liquid-phase hydrogenation of benzene to cyclohexene over Ru–B/ZrO_2 catalysts. *Ind. Eng. Chem. Res.*, 2012, **5**, 12205−12213.

42 H. J. Sun, Y. J. Pan, H. B. Jiang, S. H. Li, Y. X. Zhang and S. C. Liu, Effect of transition metals (Cr, Mn, Fe, Co, Ni, Cu and Zn) on the hydrogenation properties of benzene over Ru-based catalyst. *Appl. Catal. A-Gen.*, 2013, **464-465**, 1−9.

43 H. J. Sun, Y. Y. Dong, S. H. Li, H. B. Jiang, Y. X. Zhang, Z. Y. Liu and S. C. Liu, The role of La in improving the selectivity to cyclohexene of Ru catalyst for hydrogenation of benzene. *J. Mol. Catal. A-Chem.*, 2013, **368-369**, 119−124.

44 H. Nagahara, M. Ono, M. Konishi and Y. Fukuoka, Partial hydrogenation of benzene to cyclohexene. *Appl. Surf. Sci.*, 1997, **121/122**, 448−451.

45 J. L. Liu, Y. Zhu, J. Liu, Y. Pei, Z. H. Li, H. Li, H. X. Li, M. H. Qiao and K. N. Fan, Discrimination of the roles of $CdSO_4$ and $ZnSO_4$ in liquid phase hydrogenation of benzene to cyclohexene. *J. Catal.*, 2009, **268**, 100−105.

46 J. Struijk, R. Moene, T. v. d. Kamp and J. J. F. Scholten, Partial liquid-phase hydrogenation of benzene to cyclohexene over ruthenium catalysts in the presence of an aqueous salt solution *Appl. Catal. A-Gen.*, 1992, **89**, 77−102.

47 H. J. Sun, Z. H. Chen, W. Guo, X. L. Zhou, Z. Y. Liu and S. C. Liu, Effect of organic additives on the performance of nano-sized Ru-Zn catalyst. *Chin. J. Chem.*, 2011, **29**, 369−373.

48 J. Struijk and J. J. F. Scholten, Selectivity to cyclohexenes in the liquid phase hydrogenation of benzene and toluene over ruthenium catalysts, as influenced by reaction modifiers. *Appl. Catal. A-Gen.*, 1992, **82**, 277−287.

49 G. Y. Fan, R. X. Li, X. J. Li and H. Chen, Effect of organic additives on partial hydrogenation of benzene. *Catal. Commun.*, 2008, **9**, 1394−1397.

50 E. V. Spinacé and J. M. Vaz, Liquid-phase hydrogenation of benzene to cyclohexene catalyzed by Ru/SiO_2 in the presence of water–organic mixtures. *Catal. Commun.*, 2003, **4**, 91−96.

51 H. J. Sun, H. B. Jiang, S. H. Li, Y. Y. Dong, H. X. Wang, Y. J. Pan, S. C. Liu, M. S. Tang and Z. Y. Liu, Effect of alcohols as additives on the performance of a nano-sized Ru–Zn(2.8%) catalyst for selective hydrogenation of benzene to cyclohexene. *Chem. Eng. J.*, 2013, **218**, 415-424.

52 P. S. Campbell, C. C. Santini, F. Bayard, Y. Chauvin, V. Collière, A. Podgoršek, M. F. C. Gomes and J. Sá, Olefin hydrogenation by ruthenium nanoparticles in ionic liquid media: Does size matter? *J. Catal.*, 2010, **275**, 99−107.

53 S. D. Miao, Z. M. Liu, B. X. Han, J. Huang, Z. Y. Sun, J. L. Zhang and T. Jiang, Ru Nanoparticles immobilized on montmorillonite by ionic liquids: a highly efficient heterogeneous catalyst for the hydrogenation of benzene. *Angew. Chem. Int. Ed.*, 2006, **45**, 266−269.

54 E. T. Silveira, A. P. Umpierre, L. M. Rossi, G. Machado, J. Morais, G. V. Soares, I. J. R. Baumvol, S. R. Teixeira, P. F. P. Fichtner and J. Dupont, The partial hydrogenation of benzene to cyclohexene by nanoscale ruthenium catalysts in imidazolium ionic liquids. *Chem. Eur. J.*, 2004, **10**, 3734−3740.

55 H. Z. Liu, S. G. Liang, W. T. Wang, T. Jiang and B. X. Han, The partial hydrogenation of benzene to cyclohexene over Ru–Cu catalyst supported on ZnO. *J. Mol. Catal. A: Chem.*, 2011, **341**, 35–41.

56 H. Z. Liu, T. Jiang, B. X. Han, S. G. Liang, W. T. Wang, T. B. Wu and G. Y. Yang, Highly selective benzene hydrogenation to cyclohexene over supported Ru catalyst without additives. *Green Chem.*, 2011, **13**, 1106−1109.

57 X. H. Yan, Q. Zhang, M. Q. Zhu and Z. B. Wang, Selective hydrogenation of benzene to cyclohexene over Ru−Zn/ZrO_2 catalysts prepared by a two-step impregnation method. *J. Mol. Catal. A: Chem.*, 2016, **413**, 85−93.

58 H. J. Sun, H. X. Wang, H. B. Jiang, S. H. Li, S. C. Liu, Z. Y. Liu, X. M. Yuan and K. J. Yang, Effect of $(Zn(OH)_2)_3(ZnSO_4)(H_2O)_5$ on the performance of Ru–Zn catalyst for benzene selective hydrogenation to cyclohexene. *Appl. Catal. A-Gen.*, 2013, **450**, 160−168.

59 H. Nagahara and M. Konishi, Process for producing cycloolefins. 1988, United States Patent EP 220525 A1 19870506.

60 G. B. Zhou, R. F. Dou, H. Z. Bi, S. H. Xie, Y. Pei, K. N. Fan, M. H. Qiao, B. Sun and B. N. Zong, Ru nanoparticles on rutile/anatase junction of P25 TiO_2: Controlled deposition and synergy in partial hydrogenation of benzene to cyclohexene. *J. Catal.*, 2015, **332**, 119−126.

61 T. Kawai, J. K. M. Jiang and T. Ishikawa, FT-IR and TPD studies of adsorbed pyridine on Re_2O_7/Al_2O_3 catalysts. *J. Catal.*, 1996, **159**, 288−295.

62 J. Wang, H. Y. Chen and Q. Z. Li, Influence of the Brönsted and Lewis acid sites in platinum/solid acid catalysts on the hydrogenation of benzene and toluen. *React. Kinet. Catal. Lett.*, 2000, **69**, 277−284.

View Article Online
DOI: 10.1039/C6TA08529F

Table of Contents

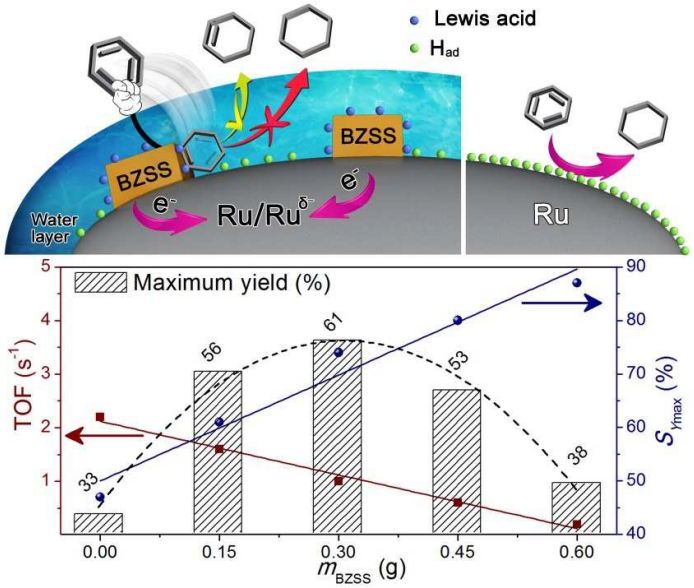

Ru active sites armed with surface BZSS nanoclusters induced high selectivity and yield for benzene-selective hydrogenation reaction. The surface-modified Ru catalyst operated stably more than 600 h on an industrial production line.